Time-lapse attenuation variations during CO_2 injection using DAS VSP data from the CaMI Field Research Station, Alberta, Canada

Yichuan Wang and Donald C. Lawton, University of Calgary and Carbon Management Canada*

Summary

For seismic monitoring injected CO_2 during geologic CO_2 sequestration, it is useful to measure time-lapse variations of seismic attenuation. Seismic attenuation directly connects to different petrophysical parameters of a CO_2 storage reservoir. We have used an approach for measuring attenuation by iteratively identifying sparse strongest reflections in the seismic trace and stacking their waveforms. This method is straightforward and requires no sophisticated inverse algorithm. It is data-driven and applied to distributed acoustic sensing (DAS) vertical seismic profile (VSP) data from the CaMI Field Research Station in Newell County, Alberta, Canada. High-quality attenuation-quantity images are obtained. Higher attenuation and time-lapse attenuation variations around the injection zone are observed, which is interpreted as being related to the injected CO_2.

Introduction

Seismic attenuation causes wave-amplitude decay during seismic wave propagation. Compared with velocity or density, attenuation is more sensitive to changes in clay content, gas or water saturation, permeability, pore fluid, and microfracturing. Attenuation can be estimated from different kinds of data such as vertical seismic profile (VSP), crosswell, sonic log or surface seismic records. In this study, we estimate attenuation parameters from distributed acoustic sensing (DAS) VSP data for monitoring injected CO_2 at the Field Research Station (FRS) established by the Containment and Monitoring Institute (CaMI).

The CaMI FRS is located in Newell County, Alberta, Canada (Figure 1a). At the FRS, we focus on the development of subsurface and surface measurement, monitoring and verification technologies for carbon capture and secure storage. There is one CO_2 injection well and two observation wells (OBS1 and OBS2, Figure 1b) at the FRS. Different geophysical instruments are permanently installed at the FRS, such as DAS using straight and helically-wound fibre optic cables with a continuous loop of about 5 km in a horizontal trench and in two observation wells (Lawton et al., 2019). Different DAS VSP surveys have been acquired at the FRS, and the monitor DAS VSP survey in this report was acquired on March 1st, 2021. Figure 1b shows the shot locations of one walk-around and three walk-away lines of this monitor survey, and this report measures the attenuation for walk-away VSP data acquired along Line 13 and Line 15. The baseline DAS VSP survey before any CO_2 injection was acquired in May 2017 for the walk-away Line 13.

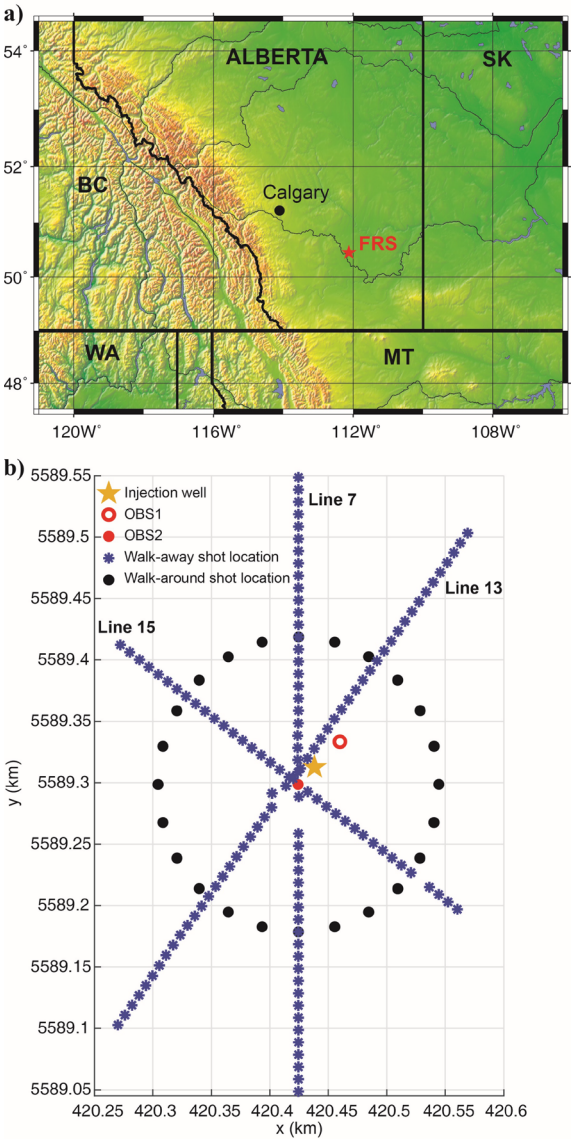

Figure 1: CaMI FRS seismic monitoring project: (a) location map in Alberta, Canada, (b) VSP layout map of the survey acquired on March 1st, 2021.

There were accumulative ~34 tonnes of CO_2 injected at the FRS prior to the monitor VSP acquisition date of March 1st, 2021. The Basal Belly River Sandstone (BBRS) is the target formation for CO_2 injection at the FRS. This formation is composed of fine to medium-grained sandstone with the

thickness of 7 m (~295 to 302 m in depth; Macquet et al., 2019). The BBRS injection zone is sealed from above by the Foremost Formation which is composed of clay sandstone of 152 m thickness (Macquet et al., 2019). This report is based on the DAS data from the down-loop and up-loop straight fibre of OBS2. Figure 2 shows the separation of upgoing (reflection) wavefield from the raw data of monitor DAS VSP survey by the application of a median and an FK filter. We measure attenuation from the time-frequency variant amplitude of stacked reflection signal. Such time-variant spectra are derived by applying Wang and Morozov's (2020) approach of identifying and stacking locally strongest reflection peaks. We demonstrate how this attenuation measurement from the DAS VSP data can help to detect injected CO_2 at the FRS.

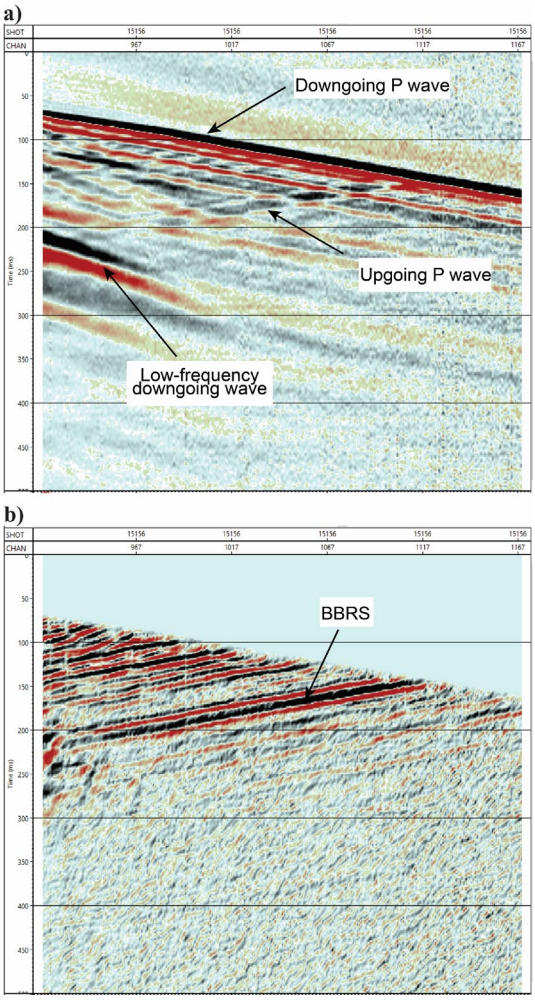

Figure 2: a) Raw DAS shot gather from the sum of data from down-loop and up-loop straight fibre of OBS2, and b) isolated P-wave upgoing wavefield.

Attenuation model and measurement

In the frequency domain, the non-stationary convolutional model for seismic reflection signal is

$$A(t,f) = S(f)R(t,f)F(t,f)G(t), \qquad (1)$$

where $A(t,f)$ is the time-frequency variant amplitude of the reflected signal recorded at the surface, $S(f)$ is the spectrum of the seismic source, $R(t,f)$ is the time-frequency response of the reflectivity, and $F(t,f)$ and $G(t)$ are the path effects on the signal spectra. $F(t,f)$ is commonly associated with seismic attenuation and related to the factor Q of the medium as $F(t,f) = \exp\left[-\pi f \int_0^t Q^{-1}(\tau)d\tau\right]$. $G(t)$ can be interpreted as the effect of focusing or defocusing, and exponentially varies as $G(t) = \exp\left[-\int_0^t \gamma(\tau)d\tau\right]$, where γ is a geometric counterpart for Q^{-1} (Morozov, 2008).

With the assumption of $R(t,f) = const$, the "apparent" attenuation parameters γ_A and Q_A^{-1} can be inverted for by first taking the logarithm and then the time derivative of equation 1:

$$\gamma_A + \pi f Q_A^{-1} = -\frac{\partial \ln A(t,f)}{\partial t}. \qquad (2)$$

Thus, if $A(t,f)$ is available, γ_A and Q_A^{-1} at time t are obtained as the coefficients of linear regression with respect to variable f in equation 2. The smooth estimates of $A(t,f)$ are derived by Wang and Morozov's (2020) approach. In this approach, a sparse set of locally strongest reflection peaks is first identified within the seismic trace and then stacked as described below.

Considering a reflected signal $u(t)$, we first identify within it a series of sparse strongest peaks at times t_j, where j is the number of selected peaks. For each peak j, we extract a waveform $w_j(\tau)$ centered at the peak. Then, at any time t_i, we extract a segment i of length T centered on t_i from $u(t)$ and consider all peaks j located within this segment. All $w_j(\tau)$ within each segment i are stacked to produce the source waveform at time t_i (Wang and Morozov, 2020):

$$s(t_i,\tau) = c_0 \sum_{j \in \text{segment } i} h\left(\frac{t_j - t_i}{T}\right) w_j(\tau), \qquad (3)$$

where factor c_0 scales the peak amplitude to $s(t_i,\tau) = 1$. The Hann time window h of the same length T with segment i apply weights to $w_j(\tau)$ located within different parts of the segment i. Therefore, the waveform $s(t_i,\tau)$ and its spectrum $S(t_i, f)$ are insensitive to segment edges. The temporal

resolution of the resulting spectra can be estimated as the half segment length $T/2$.

Due to the scaling procedure as in equation 3, the amplitude variation from the original signal $u(t)$ is distorted. To correct this effect, we first normalize the spectrum $S(t_i, f)$ of the waveform $s(t_i, \tau)$ from equation 3 so that the root-mean-square (RMS) amplitude of the normalized spectrum equals to one. This normalized spectrum is denoted as $\overline{S}(t_i, f)$. We then measure the RMS amplitude of each segment i from record $u(t)$, denoted as $u_i^{\text{rms}}(t_i)$. The time-variant spectra for attenuation measurements from equation 2 are obtained as

$$A(t_i, f) = u_i^{\text{rms}}(t_i)\,\overline{S}(t_i, f). \quad (4)$$

Results

We first measure the attenuation parameters from monitor VSP common depth-point (CDP) stack from walk-away Line 15. The northwest-southeast Line 15 crosses OBS2 and is perpendicular to well layout with a 20 m perpendicular distance to injection well (Figure 1b). The VSP CDP stack is obtained from the isolated upgoing reflections of each shot gather as in Figure 2. Figure 3 shows the monitor VSP CDP stack of high quality with the BBRS reflection indicated, and the measured differential attenuation quantities γ_A and Q_A^{-1} from the time derivative of $A(t, f)$ (equation 2). There is higher attenuation around OBS2 at the BBRS zone with the Q_A^{-1} value around 0.06, which should be related to increased CO_2 saturation and/or pore pressure.

Figure 4 then shows the measured Q_A^{-1} from baseline and monitor VSP CDP stack from walk-away Line 13, and the attenuation difference calculated by subtracting the baseline Q_A^{-1} from the monitor Q_A^{-1}. The Line 13 length from baseline is around one fifth shorter than from monitor. The southwest-northeast Line 13 in Figure 1b is parallel with well layout, and adjacent to OBS2 at CDP 62 as shown by black dashed line in Figure 4. The measurement from baseline data (Figure 4a) shows there is no attenuation anomaly around the BBRS target zone before CO_2 injection and the measurement from monitor data (Figure 4b) shows higher attenuation around the BBRS with the largest Q_A^{-1} value ~0.08. This attenuation anomaly from monitor data is on the southwestern side of injection well. The highest attenuation shown on the southwestern side of OBS2 and not around the injection well could be related to the gas-phase CO_2, which should be at the leading edge of the CO_2 plume. The calculated attenuation difference in Figure 4c also shows an increase of attenuation on the southwestern side of injection well during CO_2 injection.

We also investigate the correlation between attenuation anomaly (larger Q_A^{-1}) from Line 15 and Line 13. As Line 15 crosses OBS2 in Figure 1b and the location of OBS2 is adjacent to CDP 62 of Line 13 in Figure 4, the attenuation anomaly from Line 15 around OBS2 (Figure 3b) is at the same location with the attenuation anomaly from Line 13 at CDP 62 (Figure 4b). The measured Q_A^{-1} values from Line 13 and Line 15 at this location are consistent and both ~0.06. This indicates that our approach can obtain stable attenuation measurement from field data such as DAS VSP.

Discussion

The errors of estimated Q and γ from seismic data are always significant, and they trade off with the available bandwidth and the desired temporal resolution (White, 1992). In this section, we estimate these errors and the temporal resolution limits for the attenuation measurement of this study.

As noted by White (1992) and recently by Wang and Lawton (2022), the measurement errors for estimated $q = Q^{-1}$ and γ are

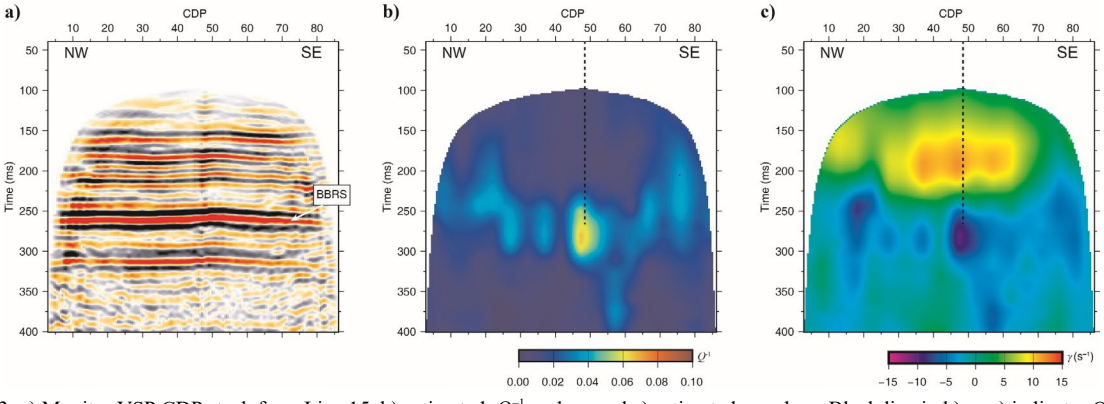

Figure 3: a) Monitor VSP CDP stack from Line 15, b) estimated Q_A^{-1} values and c) estimated γ_A values. Black line in b) or c) indicates OBS2.

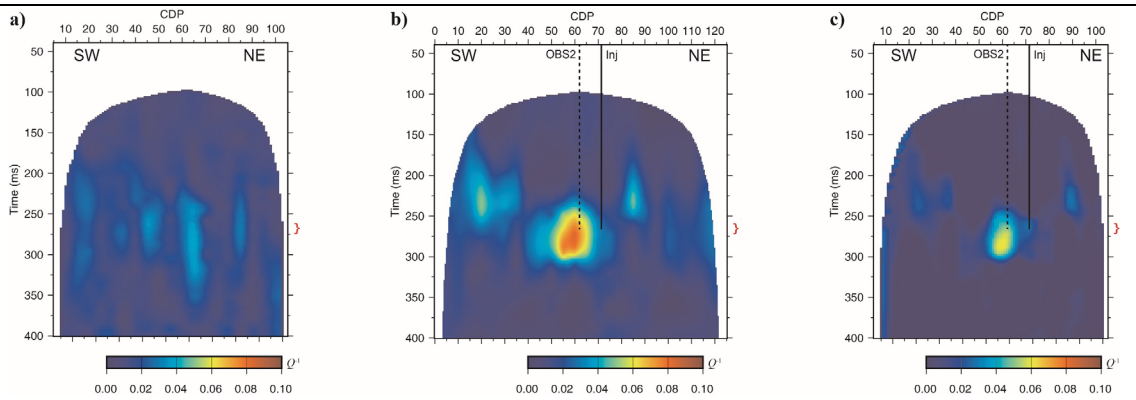

Figure 4: Estimated Q_A^{-1} from Line 13 from a) baseline and b) monitor VSP CDP stack, and c) attenuation difference. Black dashed or solid line indicates the OBS2 or CO_2 injection well, respectively. The BBRS injection zone is indicated by the red brackets.

$$s_{\hat{\gamma}} = \frac{1}{\sqrt{2}\Delta t}\frac{1}{\sqrt{BT_w}} \text{ and } s_{\hat{q}} = \frac{s_{\hat{\gamma}}}{\pi cB} = \frac{1}{\pi\sqrt{2}c}\sqrt{\frac{1}{BT_w}}\frac{1}{B\Delta t}, \quad (5)$$

where T_w is the length of each waveform $w_j(\tau)$ in spectral measurement (equation 3), B is the signal frequency bandwidth, c is a proportional factor between RMS average of demeaned frequencies and signal bandwidth, and Δt is the temporal resolution. In this study, Δt is measured as half length of the Hann time window used in equation 3: $\Delta t = T/2$.

In Figure 5, we evaluate the relative errors $e_{\hat{q}} = s_{\hat{q}}/\hat{q}$ and $e_{\hat{\gamma}} = s_{\hat{\gamma}}/|\hat{\gamma}|$ as the ratio of errors from equations 5 of different Δt and the different values of estimated $\hat{q}$ and $\hat{\gamma}$. From Figure 5, we can observe a significant trade-off between the accuracy of estimated $\hat{q}$ or $\hat{\gamma}$ and the temporal resolution Δt. For $\Delta t = 200$ ms (the black dashed lines in Figure 5) used in this study, the estimated $\hat{q}$ needs to be larger than ~0.09 and the estimated $|\hat{\gamma}|$ needs to be larger than ~6.5 s^{-1} for achieving an error lower than 30%. For the typical large value of $\hat{q} = 0.08$ and $|\hat{\gamma}| = 10$ s^{-1} (the black solid lines in Figure 5) around the BBRS injection zone, the relative errors under $\Delta t = 200$ ms are modest $e_{\hat{q}} \approx 34\%$ and $e_{\hat{\gamma}} \approx 20\%$. However, for the non-injection zones with much smaller $\hat{q}$ and $\hat{\gamma}$, the relative errors are significantly larger even with much lower resolution.

Conclusion

Attenuation parameters of both Q^{-1} and its geometric counterpart γ are measured from the DAS VSP data at the CaMI FRS for monitoring CO_2 injection. High attenuation with significant Q^{-1} values and increases of Q^{-1} are shown at the CO_2 injection zone and correlated with the injection well. The attenuation measured through the approach of identifying and stacking sparse strongest reflections can be reliable CO_2 indicator for CCS monitoring.

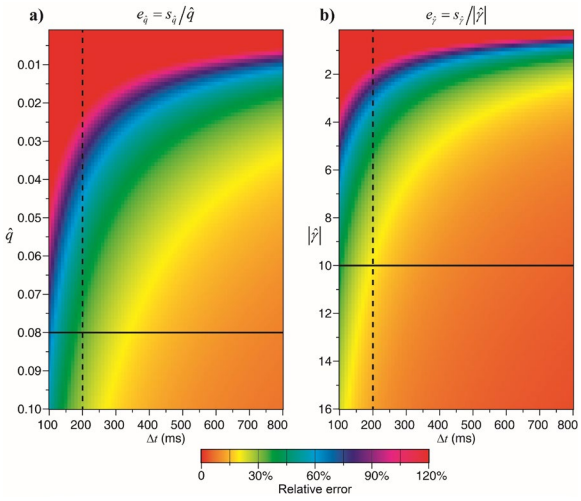

Figure 5: Relative errors of estimated (a) $\hat{q}$ and (b) $\hat{\gamma}$.

Acknowledgments

Research at the CaMI field site is supported in part by the CFREF (Canada First Research Excellence Fund), through the GRI (Global Research Initiative) at the University of Calgary. We thank the CaMI.FRS Joint Industry Project members and CREWES sponsors for continued support. We also acknowledge support from NSERC (Natural Science and Engineering Research Council of Canada) through the grant CRDPJ 543578-19.